Atmos. Chem. Phys. Discuss., 12, 5247–5292, 2012
www.atmos-chem-phys-discuss.net/12/5247/2012/
doi:10.5194/acpd-12-5247-2012

Atmospheric Chemistry and Physics Discussions

The effect of ENSO-induced rainfall and circulation changes on the direct and indirect radiative forcing from Indonesian biomass-burning aerosols

A. Chrastansky and L. D. Rotstayn

CSIRO Marine and Atmospheric Research, Aspendale, Vic, Australia

The Centre for Australian Weather and Climate Research. A partnership between CSIRO and the Bureau of Meteorology, Australia

Received: 10 January 2012 – Accepted: 6 February 2012 – Published: 17 February 2012

Correspondence to: A. Chrastansky (alena.chrastansky@csiro.au)

Published by Copernicus Publications on behalf of the European Geosciences Union.

Abstract

Emissions of biomass-burning aerosols from the Indonesian region are known to vary in response to rainfall anomalies associated with the El Niño Southern Oscillation (ENSO). However, the effects of these rainfall anomalies on regional aerosol burdens and radiative forcing have not been investigated. In this study, we simulate the effects of ENSO-related changes in (1) emissions and (2) rainfall and circulation on the radiative forcing of Indonesian biomass-burning aerosols. We find that rainfall and circulation anomalies, as well as emissions, contribute substantially to the direct and first indirect radiative effects.

We compare two experiments that are performed with the CSIRO-Mk3.6 atmospheric global climate model (GCM). The first experiment (AMIP) consists of a pair of runs that respectively represent El Niño and La Niña conditions. In these runs, the distribution of aerosols is simulated under the influence of realistic Indonesian biomass-burning aerosol emissions and sea surface temperatures (SSTs) for 1997 (El Niño) and 2000 (La Niña). The second experiment (CLIM) is identical to AMIP, but is forced by climatological SSTs, so that in CLIM meteorological differences between 1997 and 2000 are suppressed.

The comparison of AMIP and CLIM shows that the radiative forcing anomalies associated with ENSO (El Niño minus La Niña) are substantially stronger when ENSO-related SST anomalies are taken into account. This is true for both for the direct and the first indirect effects. SST-induced changes in rainfall and wind fields enhance the anomaly of aerosol burdens over Indonesia and the equatorial Indian Ocean. This, in turn, has an indirect effect on cloud properties due to changes in the concentration and radii of cloud droplets.

Our results suggest that the direct and indirect radiative effects of Indonesian biomass-burning emissions would be underestimated if feedbacks of ENSO-related SST variations on radiative forcing are not taken into account.

ACPD
12, 5247–5292, 2012

1 Introduction

In the Indonesian region, high fire activity occurs in response to negative precipitation anomalies. These usually occur during the El Niño phase of the El Niño Southern Oscillation (ENSO). During the La Niña phase, fire activity is suppressed due to increased rainfall. Several studies have shown that enhanced emissions of biomass burning (BB) aerosols during El Niño exert substantial effects on regional radiative forcing (Duncan et al., 2003; Davison et al., 2004; Rajeev et al., 2008).

ENSO has a large influence on the climate of the Indonesian region. These quasi-periodic variations of sea surface temperature (SST) in the equatorial Pacific change regional atmospheric dynamics. During El Niño events, warm SST anomalies prevail in the central Pacific, while SSTs around Indonesia are cooler than normal. During La Niña the situation changes to the contrary, with cool SST anomalies in the central Pacific and warm SST anomalies around Indonesia. This causes a shift of the Walker circulation, so that the Indonesian region experiences decreased precipitation rates during El Niño events and increased rainfall in La Niña conditions.

Drier conditions in Indonesia are welcome for farmers and landowners with respect to land clearing. Fires are a common tool for land clearing in this region and are often deliberately set in the dry season (Murdiyarso and Adiningsih, 2007). During extended droughts the risk of a fire spreading increases and fires sometimes end up raging for several months. In such cases, large amounts of trace gases and aerosols are emitted. In 1997, for example, one of the strongest El Niño events of the past century occurred. This went along with severe droughts in the Indonesian region, which considerably promoted fire activity. A strong Indian Ocean Dipole coincided with the 1997 El Niño, which might have contributed to the very dry conditions in Indonesia (Saji et al., 1999; Webster et al., 1999). As a result, intense fires occurred predominantly in the main islands of Indonesia, such as Sumatra and Borneo (Duncan et al., 2003; Liew et al., 1998), leading to exceptionally high aerosol loads in the Indonesian region (Levine, 1999; Parameswaran et al., 2004; van der Werf et al., 2010). Page et al. (2002), for

ACPD
12, 5247–5292, 2012

instance, estimated that during the 1997 El Niño between 0.8 and 2.6 Pg of carbon has been released from fires in Indonesian peatlands. Van der Werf (2010) gave an estimate of 1069 Tg C for equatorial Asia, which lies well within the range of Page et al. (2002).

Based on detailed emission estimates such as those provided by the Global Fire Emission Database (GFED) (van der Werf et al., 2010) it is possible to simulate the distribution of aerosols using regional or global climate models (GCMs). Besides simulating the transport and removal of aerosols, these models enable calculation of the effects such BB events may have on regional climate. Aerosols scatter and absorb short-wave (SW) radiation and thus directly influence the regional radiation budget. Tosca et al. (2010), for instance, investigated the radiative impact of the 1997 Indonesian fires using an atmospheric GCM coupled to a slab ocean model. They concluded that the 1997 fires substantially affected the radiation budget over the main islands of Indonesia, namely Sumatra and Borneo. Comparing the 1997 to year-2000 La Niña conditions, they stated that incoming SW radiation was reduced by around 19 $W m^{-2}$ at the surface during the months of August to October, with largest impacts occurring in September ($-25 W m^{-2}$). Simultaneously, absorbing components led to atmospheric heating (21 $W m^{-2}$) during the dry season. Other studies had a closer look at the spatial variation of SW reductions. Strongest impacts occurred locally close to the burning regions with SW reductions at the surface between -150 to $-200 W m^{-2}$ when aerosol loads were highest (Davison et al., 2004; Duncan et al., 2003; Podgorny et al., 2003). The direct impact (SW scattering and absorption) of the 1997 aerosol haze reached far beyond Indonesia, so that surface radiation was reduced by 10 $W m^{-2}$ over large areas of the tropical Indian Ocean (Duncan et al., 2003).

Direct scattering and absorption of solar radiation is not the only way in which aerosols can influence the climate. Aerosols also have the ability to change cloud properties by acting as cloud condensation nuclei (Ramanathan, 2001). Assuming that the liquid water content in a cloud remains unchanged and that water tends to distribute equally over the number of cloud droplets, an increase in the number of cloud

ACPD
12, 5247–5292, 2012

droplets would result in smaller droplet radii. This increases cloud albedo and more solar radiation will be reflected back to space (Twomey, 1974). Increased cloud albedo also results in a reduction of available solar radiation at the surface. Until now, the cloud-albedo effect (also referred to as the first indirect effect) has not been considered in studies dealing with Indonesian biomass burning.

The magnitude of aerosol forcing is strongly connected to the amount of aerosols released into the atmosphere. Resulting aerosol burdens, in turn, are dependent on aerosol transport and removal. When precipitation is reduced, for example, aerosols are less effectively scavenged by rain, which might have a positive feedback on aerosol burdens. Another influencing factor is the horizontal transport of aerosols by wind. Since in the Indonesian region ENSO has an impact on both, we expect that changed atmospheric conditions will have a non-negligible effect on radiative perturbations from Indonesian BB. To our knowledge there has been no attempt to analyse the extent to which radiative forcing is increased by ENSO-related rainfall variations.

To address this question, we performed two GCM-experiments, in which we quantified radiative perturbations caused by Indonesian BB aerosols with and without the influence of ENSO-related SST anomalies. Our main focus is on the strong 1997 El Niño, which has been investigated in several other studies. We consider the direct and first indirect aerosol effects individually. The current study demonstrates that both the direct and first indirect radiative effect are substantially enhanced when the impact of ENSO-related SSTs on climatic conditions are taken into account.

2 Method

Two experiments were performed using the CSIRO Mark 3.6 (Mk3.6) atmospheric Global Climate Model (GCM). The model is described in Sect. 2.1. Details about the experimental design can be found in Sect. 2.2.

ACPD
12, 5247–5292, 2012

2.1 Model description

The Mk3.6 GCM has a horizontal resolution of $1.9^\circ \times 1.9^\circ$ (T63) and 18 vertical levels in the atmosphere. It is developed from the Mk3.5 model, which has been described in detail by Gordon et al. (2010). The main differences between Mk3.5 and Mk3.6 are an interactive aerosol and an updated radiation scheme in the latter version. A brief summary is given in Rotstayn et al. (2010).

The aerosol scheme of Mk3.6 includes eleven prognostic variables, namely dimethyl sulphide (DMS), sulphur dioxide (SO_2), sulphate (SO_4), hydrophobic and hydrophilic forms of black carbon (BC) and organic carbon (OC), as well as four size bins of mineral dust (radii ranging from 0.1–1, 1–2, 2–3 and 3–6 µm). Sea salt (film-drop and jet-drop) is diagnosed as a function of the 10 m-wind speed above the ocean surface (O'Dowd et al., 1997) but is not treated prognostically.

The emissions of anthropogenic and BB aerosols (i.e. SO_2 and carbonaceous aerosols) are prescribed and taken from the Coupled Model Intercomparison Project Phase 5 (CMIP5) (Lamarque et al., 2010). BB emissions from the Indonesian region (5.6° N–11.2° S, 96.6° E–150.9° E) are taken from the Global Fire Emission Database version 3 (GFED3) (van der Werf et al., 2010). Note that yields of secondary organic aerosols due to gas-to-particle conversion are not included in GFED3 aerosol estimates. Depending on the climatic zone, BB emissions are injected into model layers following emission height distributions in Dentener et al. (2006). In the tropics, for instance, 20 % of the BB emissions are emitted in the lowest model layer to an altitude of 100 m, and the remaining 80 % are evenly distributed in higher levels up to 1000 m.

The treatment of sulphur chemistry is based on that in ECHAM4 (Feichter et al., 1996) with some modifications as in Rotstayn and Lohmann (2002). It describes the transformation due to oxidation involving sulphate precursors. For carbonaceous aerosols (BC and OC), the decay from their hydrophobic forms into their hydrophilic forms follows the approach of Cooke et al. (1999), assuming an e-folding decay-time of one day for the conversion. Particles containing black and organic carbon are

ACPD
12, 5247–5292, 2012

assumed to exist as an internal mixture. All others are assumed to form externally mixed aerosols.

Prognostic aerosol species are transported by advection and sub-grid turbulent and convective mixing, and removed from the atmosphere by dry and wet deposition. Vertical advection is handled using a flux-corrected transport scheme (van Leer, 1977), and horizontal advection follows a semi-Lagrangian scheme (McGregor, 1993). Parametrization of vertical turbulent mixing is based on the Louis (1979) stability-dependent mixing scheme. An additional non-local counter-gradient flux (Holtslag and Boville, 1993) is added when convective conditions occur. Vertical transport is based on the updraft mass flux and compensating subsidence from the convection scheme (Gregory and Rowntree, 1990).

Aerosols are removed from the atmosphere by wet and dry depositions. In-cloud and below-cloud wet-scavenging of aerosols are linked to precipitation processes in the stratiform cloud microphysical scheme (Rotstayn, 1997; Rotstayn and Lohmann, 2002) and the convection scheme (Gregory and Rowntree, 1990). Dry deposition processes are based on Lohmann et al. (1999) for SO_4, SO_2 and carbonaceous aerosols. For dust, dry deposition and gravitational settling follows the formulation of Ginoux et al. (2001).

The radiation scheme covers direct and indirect aerosol radiative effects and involves SW effects from all aerosols as well as long wave effects of dust and volcanic aerosol (Rotstayn et al., 2007, 2011). The latter, however, was set to zero for the purpose of this study. We also suppressed changes in cloud lifetime due to aerosol-induced changes in precipitation efficiency by setting $N_d = 100 \times 10^6$ m^{-3} in the rain-formation parameterization in the cloud scheme (Rotstayn and Liu, 2005). The treatments of the first aerosol effect (Twomey, 1977) is included in the cloud scheme of Mk3.6. Based on the number concentration of hydrophilic aerosols (A in m^{-3}), i.e. sulfate, sea salt and hydrophilic carbonaceous aerosol, the cloud droplet number concentration of liquid-water clouds (N_d in m^{-3}) is determined as follows (Jones et al., 1994):

$$N_d = \max\left\{375 \times 10^6 \left(1 - e^{-2.5\times10^{-9}\mathrm{A}}\right), N_{d_{min}}\right\}, \quad (1)$$

ACPD
12, 5247–5292, 2012

where $N_{d_{min}} = 10 \times 10^6\,m^{-3}$.

The cloud effective radius R_e (in m) is dependent on N_d and the cloud liquid water content L (in $kg\,m^{-3}$) (Rotstayn and Liu, 2003):

$$R_e = \beta \left(\frac{3L}{4\pi\rho_l N_d} \right)^{\frac{1}{3}} \quad (2)$$

where ρ_l is the density of liquid water and β the spectral shape factor. The parametrization of β follows an empirical relationship from Liu et al. (2008), accounting for variations in L and N_d ($\beta = 0.07 \times (L/N_d)^{-0.14}$) (Rotstayn et al., 2009).

2.2 Experimental design

We performed two pairs of runs, each pair consisting of an El Niño and a La Niña simulation. In the El Niño simulation BB emissions from the Indonesian region (5.6° N–11.2° S, 96.6° E–150.9° E) are set to the year 1997 and for the La Niña simulation to the year 2000. For all other aerosol emissions (including BB emissions from regions other than Indonesia) both runs use year-2000 emissions from CMIP5. The BB emission estimate from CMIP5 for the year 2000 is representative for the decade 1997 to 2006 and deliberately doesn't try to resolve events such as El Niño (Lamarque et al., 2010).

For the first pair of runs (hereafter "CLIM") climatological SSTs are used. Hence, SST forcing is identical in the El Niño and La Niña runs of CLIM. For the second pair of runs (hereafter "AMIP") we use realistic SSTs for the year 1997 in the El Niño simulation and SSTs for the year 2000 in the La Niña simulation. The SST fields for the AMIP runs are taken from the Atmospheric Model Intercomparison Project (Hurrell et al., 2008).

A short summary of the most important characteristics of CLIM and AMIP is provided in Table 1.

In each experiment, the difference between the El Niño and the La Niña simulation gives the forcing anomaly associated with ENSO-related variations in BB emissions. Double calls to the SW radiation scheme were used to calculate the direct and first

ACPD
12, 5247–5292, 2012

indirect effects as instantaneous forcings (Lohmann et al., 2010). As described in the next paragraph, each simulation was repeated with a slightly different treatment of the double call to the SW radiation scheme, to enable calculation of the direct and indirect effects individually.

In simulations for estimating the direct forcing the indirect aerosol effect is switched off, and vice versa. For diagnosing the direct aerosol effect, both calls of the SW radiation scheme use a fixed value of cloud droplet number concentration (N_d = 100×10^6 m^{-3}), to ensure that the indirect aerosol effect is turned off. In the first call the radiation scheme "sees" the aerosols. In the second call (which affects the meteorology in the model), the direct effects of aerosols are set to zero. This implies that the meteorology remains unchanged by aerosol effects. As a result, the meteorology in the CLIM experiment is identical for the El Niño and La Niña runs.

For calculation of the first indirect effect, direct aerosol effects are turned off by setting aerosols to zero for the direct aerosol effects in both calls to the SW scheme. The first call uses N_d from Eq. (1) and the second call uses a fixed value ($N_d = 100 \times 10^6$ m^{-3}). Hence, as for the direct aerosol effect, aerosols have no impact on the meteorology, so that the meteorology is identical for the El Niño and La Niña runs in the CLIM experiment.

Note that, for the indirect effect, the differences between the SW fluxes calculated from the first and second calls in each run (say, ΔF_{1997} and ΔF_{2000}) are not physically meaningful, since the fixed value of N_d in the second call is arbitrary. However, the difference of these between the El Niño and La Niña runs ($\Delta F_{1997} - \Delta F_{2000}$) represents the indirect forcing between 1997 and 2000, due to cancellation of the fixed value of N_d. A similar method was used by Rotstayn et al. (2009) and Lohmann et al. (2010).

For the CLIM simulation we ran the model for 11 years, including a model spin-up time of one year. Except for the BB emissions from the Indonesian region, El Niño and La Niña runs were initialised with identical conditions. For the analysis we averaged over the ten years after the spin-up phase. For AMIP, we chose a longer spin-up time of 10 years (1987–1996) to let soil moisture adjust to initial conditions, and used CMIP5

ACPD
12, 5247–5292, 2012

anthropogenic and BB aerosol emissions (Lamarque et al., 2010) from the year 2000 globally. From 1997 onwards the Indonesian aerosol emissions as well as global SST fields correspond to the years 1997 to 2006. We carried out five AMIP simulations, each initialised from a different atmospheric state in 1987, so the results presented for 1997 and 2000 each represent five-member ensemble averages. The simulated period in AMIP was extended to 2006 so that the model behaviour could be compared with satellite retrievals using averaged values over the El Niño events in 2002, 2004 and 2006 and the La Niña events in 2000, 2001 and 2005, respectively. Values based on the extended (post-2000) AMIP runs will be referred to as "AMIP*".

3 Results and discussion

3.1 Aerosol emissions and burdens

The amounts of SO_2, OC and BC that were emitted from Indonesian forest fires in the El Niño year 1997 and the La Niña year 2000 differ substantially. While during the first half of the year emissions were similar in 1997 and 2000, biomass burning emissions in the second half of the year were significantly raised in 1997 (not shown). Figure 1 shows spatially averaged emission anomalies for the months July through to November. These are the months in which the GFED3 emission estimates suggest the largest anomalies. According to Fig. 1, the main contributing regions are southern Sumatra, southern Borneo (Kalimantan) and to a lesser extent the south-westerly region of New Guinea.

Increased fire emissions result in an increase of atmospheric aerosol loads. Figure 2 shows the difference of the July to November average of the SO_4, OC and BC burdens between the El Niño and the La Niña simulation from the CLIM (left column) and the AMIP (right column) experiments. In tune with the emissions, in both experiments aerosol loads are largest close to the major burning regions over south Sumatra and Kalimantan, with a second but much smaller peak over the south-western region

ACPD
12, 5247–5292, 2012

of New Guinea. West of Sumatra over the eastern equatorial Indian Ocean aerosol burdens are substantially raised. Figure 2 indicates, however, that despite the fact that the emissions are identical in CLIM and AMIP, in AMIP the aerosol loads are generally higher and reach further out into the Indian Ocean. This becomes particularly obvious when comparing the panels illustrating the sulphate burdens (panels a and b). While in CLIM anomalously high amounts of sulphate remain close to the dominating source regions of Sumatra and Borneo, in AMIP sulphate levels are raised in the entire Indonesian region, stretching from 60° E to 170° E. Carbonaceous aerosol burdens (OC and BC) are similarly enhanced.

In AMIP, additional regions appear with altered aerosol burdens, which seem not necessarily related to Indonesian biomass burning; this is explained in Sect. 3.2.

3.2 SST-induced differences in the atmospheric circulation

In both of our experiments, anomalies in aerosol distribution in the atmosphere are initiated by an El Niño-related increase of BB aerosols from the Indonesian region. How many aerosols remain in the atmosphere, however, is influenced not only by emission strengths, but also by the efficiency of aerosol removal (i.e. dry or wet deposition) and transport. Comparing the AMIP and CLIM experiments, the main differences are caused by differing rainfall and atmospheric circulation patterns induced by SST variations.

3.2.1 Rainfall patterns

Due to identical (climatological) SSTs in the CLIM experiment, the atmospheric circulation and rainfall remain unchanged in the El Niño and La Niña simulation. Hence, in the CLIM experiment the pattern of aerosol removal due to rainfall as well as the strength and direction of aerosol transport is the same in both years. This is, however, not the case in the AMIP experiment. Figure 3a shows the average rainfall anomaly (El Niño minus La Niña) of AMIP for the period July to November. Rainfall rates are substantially

ACPD
12, 5247–5292, 2012

reduced not only in the Indonesian region. In the region from 5° N and 10° S and 60° E and 165° E, rainfall is generally reduced by more than 6 mm day^{-1}. Hence, in contrast to CLIM, regions with higher BB emissions coincided with anomalously dry conditions in the AMIP experiment. Therefore, besides a larger amount of aerosols emitted into the atmosphere, aerosol removal is less efficient, so that the lifetime of aerosols is increased during El Niño.

The impact of SSTs on rainfall is also visible outside Indonesia. Over parts of India, the Bay of Bengal and the South China Sea, for instance, a positive rainfall anomaly appears in the AMIP experiment. Increased wet-scavenging of aerosols result in reduced aerosol burdens (see right column panels of Fig. 2) although by design of our experiments the emissions from these regions are equal in the El Niño and La Niña simulations. Similarly, there are positive SO_4 anomalies due to small negative rainfall anomalies over China (an area with large SO_4 emissions) and over the climatologically dry Arabian peninsula. Note that the scale used for Fig. 3 does not clearly show the small rainfall anomalies over China and the Arabian peninsula.

We compared the AMIP rainfall anomaly to the rainfall anomaly calculated from corresponding years (1997 minus 2000) of the Global Precipitation Climatology Project (GPCP) (Adler et al., 2003; Huffman et al., 2009) (Fig. 3b). The comparison indicates that Mk3.6 tends to overestimate the magnitude of the rainfall anomaly but captures the rainfall patterns in the Indonesian region very well. In the La Niña simulation of AMIP (not shown), the equatorial region (5° S to 5° N and 50° E to 180° E) appears on average about 2 mm day^{-1} too wet, while India, Thailand and the Philippines (from 5° N to 20° N , and 70° E to 140° E) are on average about 2.9 mm day^{-1} too dry. The El Niño simulation of AMIP (not shown) has similar tendencies but is closer to the GPCP estimates. In both datasets the strongest negative rainfall anomaly is located west of Sumatra in the equatorial Indian Ocean (compare Figs. 3a and 3b). While the GCPC data suggests that in this region the difference between the El Niño and La Niña year lies between −6 and −12 mm day^{-1} during the specified months, the rainfall anomaly exceeds −12 mm day^{-1} in the AMIP experiment. The GCPC rainfall anomaly indicates

ACPD
12, 5247–5292, 2012

that anomalously dry conditions were also present in the Philippines. In AMIP there is an anomaly of opposite sign, however, as the Philippines lie outside our study area this does not affect the results of this study. The general overestimation of the rainfall anomaly by AMIP could result in an overestimation of the change in wet-scavenging of aerosols in our study.

3.2.2 Wind patterns

Figure 4a shows the mean July to November 850 hPa wind fields that apply for both the El Niño and La Niña simulation of CLIM. In the entire Indonesian region easterly winds prevail with stronger winds south of the equator. CLIM wind fields are similar to the La Niña situation in AMIP; the latter indicates slightly weaker winds over the equatorial Indian Ocean and somewhat stronger winds east of New Guinea (not shown).

Figure 4b shows the 850 hPa wind anomaly (El Niño minus La Niña) from the AMIP simulation, averaged over the months July to November. There are mainly two regions in which wind changes affecting the Indonesian region become apparent. In the El Niño simulation, stronger easterly winds form west of about 120° E so that air masses from the main islands Sumatra and Borneo get directed away from Indonesia into the Indian Ocean. East of 150° E the wind anomaly indicates westerly winds, resulting from weaker easterly winds during El Niño through a weakening of the Walker Circulation. Here, the aerosol transport would be reduced.

Since the La Niña simulation in AMIP has similar winds to CLIM, wind fields in the El Niño simulations show distinct differences in AMIP and CLIM. In regions west of 120° E, easterly winds were much stronger in AMIP, so that in CLIM aerosols are likely to be much less efficiently transported away from the burning regions.

3.3 Aerosol optical depths

The anomaly of the clear-sky aerosol optical depths (AODs) averaged for the period July to November are presented in Fig. 5. As a result of differing aerosol distributions,

ACPD
12, 5247–5292, 2012

the AODs in CLIM and AMIP vary markedly. As in CLIM, the source of the BB aerosols is clearly visible, showing positive anomalies over the main burning regions and in the eastern Indian Ocean. In AMIP, however, the AOD anomaly is substantially larger and stretches further to the west into the Indian Ocean. As a result, during El Niño AODs are raised from 60° E through to about 150° E. Enhanced AODs are also visible south of the Arabian Peninsula and the Northern Arabian Sea, which are not a result of Indonesian BB. Rather, dust particles that got wind-advected from the African continent as well as rainfall-related higher SO_4 loads in 1997 lead to increases in the AODs (see Sects. 3.1 and 3.2).

We compared CLIM and AMIP clear-sky AODs at 550 nm with satellite-derived AODs from the sensors MODIS (Moderate Resolution Imaging Spectroradiometer) (King et al., 2003; Remer et al., 2005) and MISR (Multi-angle Imaging SpectroRadiometer) (Chen et al., 2008; Kahn et al., 2005). Due to a lack of data for the year 1997, we use retrievals from the El Niño years 2002, 2004 and 2006 and the La Niña years 2000, 2001 and 2005. This implies that an absolute agreement cannot be expected for 1997. For this reason, we also include monthly mean AODs based on the same El Niño (2002, 2004, 2006) and La Niña (2000, 2001, 2005) years as for the satellite data from the extended AMIP run and refer to this as "AMIP*".

Monthly averaged AODs from CLIM, AMIP and AMIP* as well as from MODIS and MISR are presented in Fig. 6. The figure indicates that AODs in the La Niña and the first half of the El Niño simulation seem to be systematically underestimated by about 0.05 to 0.1 in all model runs (CLIM, AMIP and AMIP*). During the drier months of the El Niño simulation, both CLIM and AMIP AODs lie within the range of the satellite retrievals, but AMIP* AODs remain smaller than those from MODIS and MISR throughout the drier months of El Niño. This indicates a general tendency within our model runs to underestimate AODs in the Indonesian region. Note that the 1997 El Niño event was a much stronger event than those for which satellite retrievals are available. Hence, it is likely that AODs suggested by MODIS and MISR in Fig. 6a are a rather low estimate for 1997.

ACPD
12, 5247–5292, 2012

The modelled AODs presented in this study could be underestimated, mainly because the formation of aerosols due to gas-to-particle formation is not taken into account for the emission estimates of GFED. Secondary organic aerosols (SOAs) can contribute substantially to the amount of regional aerosol loads. Grieshop et al. (2009) and Iinuma et al. (2010), for instance, stated that SOAs may increase aerosol burdens by a factor of 1.5 to 2.8. In addition, van der Werf et al. (2010) stated that the emission estimates are likely to be too low due to uncertainties in burned area estimates. Another factor that may influence AODs is the tendency of our model to overestimate rainfall in the equatorial region. Section 3.2.1 indicates, however, this is more pronounced for the La Niña simulations.

The tendency of our model to underestimate AODs is associated with an underestimate of scattering and absorption of solar radiation so that the diagnosed magnitude of aerosol direct radiative forcing is likely to be too low. The same doesn't necessarily follow for the indirect aerosol effect as this strongly depends on the model parametrization for cloud droplet number concentration.

3.4 Anomalies in the direct aerosol forcing

The direct radiative forcing anomaly for the Indonesian region (5.6° N–11.2° S, 96.6° E–150.9° E), defined as the difference between 1997 and 2000 conditions, is shown on a monthly basis in Fig. 7. In both experiments, substantial radiation anomalies are present in the months July through to November. Despite the fact that the injected aerosol emissions are identical in CLIM and AMIP, the radiative impact of raised biomass-burning aerosols shows larger impacts in the AMIP experiment.

In AMIP, the strongest difference between the El Niño and La Niña simulation occurs in September: at the surface anomalies amount to $-15\,\mathrm{W\,m^{-2}}$ while at the same time the top of atmosphere (TOA) radiation is reduced by $3\,\mathrm{W\,m^{-2}}$. In CLIM, the magnitude of the direct forcing anomaly peaks in October with about $-9\,\mathrm{W\,m^{-2}}$ at the surface and around $-2\,\mathrm{W\,m^{-2}}$ at the TOA. During the entire burning period, CLIM direct forcing anomalies remain weaker than the anomalies in AMIP. The more pronounced

ACPD
12, 5247–5292, 2012

difference between the radiative forcing at the surface and the TOA in the AMIP experiment indicates that stronger atmospheric heating due to aerosol absorption also takes place in the AMIP experiment.

Figure 8 shows the CLIM (panel a) and AMIP (panel b) direct forcing anomaly at the surface, averaged over the months September and October. This is the period of time when ENSO-related emission anomalies show the largest impact in both experiments. Panel (c) of Fig. 8 illustrates the difference between panels (b) and (a) (AMIP minus CLIM).

Although the largest radiative perturbations occur close to the source regions, El Niño-related aerosol emissions spread out and reduce surface radiation in much of the Indian Ocean and parts in the western equatorial Pacific. In both experiments, perturbations are strongest west of Sumatra in the eastern equatorial Indian Ocean. In the AMIP simulation, however, the radiative impact is substantially enhanced both in strength and spatial extent (Fig. 8c). In the eastern Indian Ocean, for instance, the area in which surface radiation is reduced by more than $10\,W\,m^{-2}$ extends further to the west and south. In a large area the magnitude of the forcing anomaly is at least $10\,W\,m^{-2}$ stronger. AMIP also shows amplified direct forcing anomalies east of 115° E, spreading in a narrow band between the equator and 5° S towards New Guinea.

Although generally weaker, the direct forcing anomaly at the TOA (left column of Fig. 9) shows a very similar pattern to the surface forcing anomaly displayed in Fig. 8. This is true for both CLIM and AMIP. The areas with strongest forcing anomalies (exceeding $-8\,W\,m^{-2}$) occur over the main emission regions. In much of the Indian Ocean a weaker anomaly ($-1\,W\,m^{-2}$ to $-2\,W\,m^{-2}$) occurs. An area of similar strength is also present in the eastern equatorial Pacific in the AMIP experiment, which does not appear in CLIM. As a result of locally increased cloudiness in AMIP south of Sumatra, BC absorption becomes apparent in a short tongue with a positive forcing anomaly of about $2\,W\,m^{-2}$.

Although AMIP direct forcing anomalies are generally stronger, panel (c) of each of the Figs. 8 and 9 indicates that close to the main source regions (i.e. southern

ACPD
12, 5247–5292, 2012

Sumatra and Kalimantan), there is an area where the direct forcing anomaly is stronger in CLIM. This is most likely caused by a weaker horizontal transport from the main emission regions of South-Sumatra and southern Borneo in the CLIM experiment (see Sect. 3.2.2).

3.5 Anomalies in the indirect aerosol forcing

The impact of increased aerosol loads during El Niño can also be seen for the indirect forcing. Figure 10 shows the anomalies of indirect forcing within the Indonesian region that are caused by aerosol-induced cloud-albedo changes. In both experiments, the magnitude of the forcing anomalies at the surface and the TOA are of similar strength. Similar to the direct forcing, the impact of increased aerosol burdens on indirect forcing is amplified in AMIP, but with a less dramatic effect on the radiation budget over Indonesia. In CLIM, changed cloud properties caused a radiation reduction mostly evident between June to November. Perturbations with the largest magnitude of $-1\,\mathrm{W\,m^{-2}}$ occurred in September. In AMIP, the indirect forcing anomalies are present throughout the year. In tune with a positive rainfall anomaly of about $0.5\,\mathrm{mm\,day^{-1}}$ during the months February and March (not shown), AMIP indirect forcing anomalies are slightly positive during this period; a more detailed explanation is given in Sect. 3.2. In the remaining months, the indirect forcing anomaly is negative, with a steep decrease from July down to $-2.9\,\mathrm{W\,m^{-2}}$ in September and October. This again gives a stronger radiative forcing than in CLIM.

The right column of Fig. 9 shows the TOA indirect forcing anomaly of CLIM, AMIP and the difference of AMIP and CLIM (panels d–f, respectively). Note that the indirect forcing anomaly at the surface looks very similar (not shown). In both CLIM and AMIP, the areas with the largest indirect forcing anomalies are located over and close to the main emission regions. The perturbations in AMIP are throughout stronger than in CLIM, reaching magnitudes of $-10\,\mathrm{W\,m^{-2}}$ and $-5\,\mathrm{W\,m^{-2}}$, respectively. Although of comparable strength and spatial scale, the pattern of the indirect radiative perturbations differs slightly from the direct forcing anomaly presented in Fig. 9. Areas in which the

ACPD
12, 5247–5292, 2012

amplification of the forcing is evident stretch in a rather narrow band from the Indian Ocean across the Indonesian region towards the western Pacific (see Fig. 9f). Unlike the direct forcing anomaly (panel c), in which stronger forcing is mostly apparent west of 110° E, the larger differences in the indirect forcing occur east of 95° E through to 170° E.

The pattern of the indirect forcing anomaly resembles the rainfall anomaly in the corresponding period (not shown), indicating a strong influence of the rainfall on the indirect forcing anomaly. This will be discussed in more detail in the following sections.

3.6 Aerosol-induced cloud property changes

3.6.1 Cloud droplet numbers

The cloud droplet number concentration (N_d) is dependent on the concentration of hydrophilic aerosols, as they are assumed to act as cloud condensation nuclei (Eq. 1). Monthly N_d anomalies for the CLIM (grey) and AMIP (black) experiments are shown in Fig. 11 together with corresponding SO_4 burdens as a surrogate for hydrophilic aerosols in the Indonesian region. In CLIM, the N_d anomaly mainly reflects the raised biomass-burning emissions from fires during El Niño. The number of cloud droplets increases slightly in June and reaches its highest anomaly in September and October with about 40 cloud droplets per cm^3. In AMIP, the N_d anomaly shows a slightly different behaviour. The number of cloud droplets increases faster so that by July the N_d anomaly from CLIM is exceeded. In September, AMIP reaches its maximum N_d anomaly with an increase of nearly 110 cloud droplets per cm^3.

Reasons for different behaviour in CLIM and AMIP are as follows. In the model it is assumed that 100 % of the sulphate aerosols are hydrophilic and 50 % of fire-emitted carbonaceous aerosols are hydrophilic when released into the atmosphere. Sulphate and the hydrophilic forms of BC and OC are efficiently wet-scavenged by rainfall (Rotstayn and Lohmann, 2002), the latter ones to a slightly lesser degree. Hence, a reduction in rainfall causes a relatively larger decrease in the removal rate of hydrophilic

ACPD
12, 5247–5292, 2012

aerosols compared to hydrophobic aerosols. Thus, the proportion of remaining hydrophilic aerosols becomes larger with decreasing rainfall in AMIP (see grey curves in Fig. 11). This also has a positive effect on aerosol lifetimes, which causes a change in the characteristics of carbonaceous aerosols. Hydrophobic carbonaceous aerosols decay into their hydrophilic forms following an e-folding time of one day, so that the proportion of hydrophilic carbonaceous aerosols increases with time. As aerosol residence times in the El Niño simulation of AMIP are longer during the drier periods, a larger number of potential cloud condensation nuclei develops.

3.6.2 Cloud droplet sizes

Figure 12 shows the monthly anomaly in cloud droplet effective radii (R_e) as a function of the N_d anomaly from the CLIM (grey) and AMIP (black) experiments. In CLIM, the rather minor increase in cloud droplets results in a similarly small decrease in the size of the cloud droplets with a maximum decrease of 0.6 µm. As the response in the number of cloud droplets is larger in AMIP, the size decrease of cloud droplets is likewise more pronounced. The R_e decrease in the Indonesian region during the months July and November, for instance, lies in AMIP between 0.5 µm and 1.8 µm. As a consequence of a larger number of smaller cloud droplets in AMIP, the cloud albedo increases so that more solar radiation is reflected back to space than in CLIM (see Sect. 3.5).

Based on estimates from CERES (Clouds and Earth's Radiant Energy System) (Minnis et al., 2011; Wielicki et al., 1996) and MODIS (King et al., 2003), we performed a comparison with R_e estimates suggested by our model results. Both datasets are based on (daytime) Terra-MODIS satellite retrievals but are processed differently. As in the AOD comparison above, we used available data covering the years 2002, 2004 and 2006 and 2000 (February to December), 2001 and 2005 for El Niño and La Niña, respectively, and completed the analysis by including R_e from the extended AMIP run (AMIP*), representing an average over the same El Niño and La Niña years as for the satellite data.

ACPD
12, 5247–5292, 2012

Although all datasets have similar differences between the seasons, CERES and MODIS R_e over the Indonesian region are generally much larger than those given by the model. While the annual averages of El Niño and La Niña lay around 10.5 µm and 10.7 µm in CLIM, 10.1 µm and 10.9 µm in AMIP and 10.5 µm and 10.9 µm in AMIP*, MODIS suggested annual averages of 17.2 µm and 17.6 µm for El Niño and La Niña, respectively. CERES annual averages are around 4 µm smaller than from MODIS, but about 3 µm larger than modelled R_e (13.3 µm and 13.4 µm during El Niño and La Niña, respectively).

A likely explanation for the smaller values of R_e in the model is that drizzle and raindrops are not included in the calculation of R_e (or radiative transfer) in the model. In common with many other GCMs, the cloud scheme in Mk3.6 uses the "autoconversion" approach, which represents the conversion of cloud droplets to precipitating drops, and the latter are assumed to rapidly fall out of the atmosphere. In contrast, the MODIS retrievals do include the effects of drizzle droplets (e.g. Suzuki et al., 2010), and these will tend to increase the retrieved droplet sizes in CERES and MODIS.

A general disagreement between R_e estimates from CERES and MODIS was also found in a study by Minnis et al. (2011). They concluded that the use of different channels, i.e. 2.1 µm in MODIS and 3.8 µm in CERES, caused a detection of larger cloud droplets in MODIS, as the vertical sampling of cloud droplets went deeper into the cloud using smaller wavelengths (Platnick, 2000). Minnis et al. (2011) also pointed out that the largest discrepancies between MODIS and CERES were present over tropical marine areas, which includes the broader Indonesian region. Note that, as stated by Minnis et al. (2011), these results suggest that smaller droplets are generally located at the cloud top, which differs from the typical adiabatic profile of non-precipitating clouds, but more research is needed to determine if the effect is real.

The monthly R_e anomalies (El Niño minus La Niña) presented in Fig. 13 show that all of the above datasets have a distinct negative R_e anomaly throughout the dry period. The maximum R_e decrease in CLIM (0.6 µm) is smaller than that from MODIS (1.2 µm), but larger than that from CERES (0.5 µm). The response in R_e seen in AMIP during the

ACPD
12, 5247–5292, 2012

drier period July to November exceeds anomalies suggested by CERES and MODIS and exhibits a largest decrease of 1.9 µm. However, the R_e anomalies from AMIP*, which are based on identical time periods as CERES and MODIS, agree fairly well with the satellite observations. Keeping in mind that the 1997 event was extraordinarily strong, the behaviour of R_e changes and consequently changes in the first indirect forcing given by our model seem to be reasonable.

3.7 Pattern correlations

To bring out the effects of SST-induced rainfall anomalies, we calculated pattern correlations based on the difference between the AMIP and CLIM anomalies (AMIP anomaly minus CLIM anomaly) for the period July to November, within the region as shown in Fig. 2. The results are summarized in Table 2. Note that rainfall represents the AMIP rainfall anomaly only as rainfall rates are identical in CLIM's El Niño and La Niña simulations.

Precipitation is most strongly correlated with N_d ($r = -0.67$), indicating the strong influence of precipitation on the amount and distribution of N_d. A slightly weaker correlation with precipitation is found for sulphate aerosols ($r = -0.62$). This is most likely a result of the positive correlation between rainfall and the liquid-water path ($r = 0.44$; not included in Table 2). Increasing rainfall tends to be associated with more liquid-water clouds, and in-cloud oxidation of SO_2 is the main source of SO_4 in the model (Rotstayn and Lohmann, 2002). This effect weakens the negative correlation between precipitation and SO_4. The impact of precipitation on OC burdens is weaker ($r = -0.49$) as it covers both its hydrophobic and hydrophilic forms. We expect, however, that the relationship of solely hydrophilic forms approximates the correlation to SO_4. Taking sulphate aerosols as a surrogate for hydrophilic aerosols, the pattern correlations of SO_4 with N_d and R_e ($r = 0.78$ and -0.67, respectively) indicate that the spatial distribution of hydrophilic aerosols strongly influences the number of cloud droplets and corresponding droplet sizes. A weaker predictor is the distribution of OC (0.65 and -0.51, respectively). As expected, the correlation between N_d and R_e is strong with

ACPD
12, 5247–5292, 2012

$r = -0.69$, and so is the correlation between precipitation and R_e ($r = -0.61$).

The rainfall pattern correlates weakly with the aerosol optical depth (τ_{550}) ($r = -0.28$). The correlation is somewhat stronger for the small particle aerosol optical depth τ_{sp} as it excludes dust and sea salt. As explained in Sect. 2.1, the latter is not treated prognostically in the model but is diagnosed solely as a function of wind speed, so it is not expected to correlate with rainfall.

The rather weak correlation of the rainfall anomaly with AODs (τ_{550} and τ_{sp}) is probably caused by an increase of relative humidity associated with more cloud and higher rainfall rates during La Niña. Increasing relative humidity tends to increase AODs and counteracts the AOD reduction due to rainfall-induced aerosol removal. Although smaller in magnitude, the correlations of τ_{550} and τ_{sp} with rainfall confirm that rainfall rates are influential for the amount of (hydrophilic) aerosols within this region. Through its consideration of both hydrophilic and hydrophobic forms, spatial changes in the aerosol optical depths (τ_{550} and τ_{sp}) correspond to a lesser extent to the increase of cloud droplets ($r = 0.47$ and 0.59) and decrease in cloud effective radii ($r = -0.38$ and -0.45). Higher SO_4 and OC burdens correlate strongly with aerosol optical depths ($r = 0.77$ and 0.76 for τ_{550}, and 0.77 and 0.90 for τ_{sp}).

3.8 Further discussion

The experiments performed for this study are idealised, in the sense that we concentrated on the direct and indirect radiative impact that appears instantaneously due to the presence of aerosols. By design, feedbacks of the aerosol radiative effects on the meteorology are not treated (see Sect. 2.2). This includes the influence on the atmospheric circulation due to surface cooling and atmospheric heating.

Rajeev et al. (2008) analysed the impact of the 1997 Indonesian smoke layer on surface temperatures in the eastern equatorial Indian Ocean. Based on SST observations, they showed that the regional changes in surface irradiance caused SSTs to drop by more than 1 °C from September to October. They stated that such substantial surface cooling through aerosols could have strengthened the prevailing Indian Ocean Dipole.

ACPD
12, 5247–5292, 2012

As SSTs used for the AMIP experiment are derived from observations (Hurrell et al., 2008), possible SST responses should generally be resolved in the AMIP simulations. Circulation changes due to atmospheric heating caused by BC aerosols, however, were not considered. This could involve stabilisation of the atmosphere (Fan et al., 2008) or locally increase vertical upward motion (Ott et al., 2010; Koch and Del Genio, 2010).

In addition, the impact of aerosols on precipitation is disregarded in this study. There is evidence, however, that Indonesian biomass-burning aerosols suppress precipitation to some degree (Graf et al., 2009; Langmann, 2007). Thus a positive feedback on the increase of aerosols can possibly be expected.

4 Summary and conclusions

This study investigated the effects of SSTs on the direct and first indirect radiative perturbations that are associated with ENSO-related variations of Indonesian BB aerosol emissions. For this purpose, two pairs of runs were performed using the CSIRO-Mk3.6 GCM, each pair consisting of an El Niño and a La Niña simulation. One experiment (CLIM) was driven by climatological SSTs, so that SSTs were identical in the El Niño and La Niña simulations. The other pair of runs (AMIP) were forced by realistic SSTs that included SST variations associated with ENSO. In both CLIM and AMIP, the difference between the El Niño and the La Niña simulation gives radiative forcing anomalies that depend on the differing fire emission strengths of the years 1997 and 2000, respectively. In the case of AMIP, SST-induced meteorological changes are also considered.

We found that SSTs have a substantial impact on the magnitude and extent of the radiative perturbations, both for the direct and the first indirect aerosol effect. The comparison of AMIP and CLIM shows that direct forcing anomalies (El Niño minus La Niña) are stronger when realistic SST variations are taken into account. The main reason is that intense BB emissions during El Niño coincide with an SST-induced negative rainfall anomaly. Drier conditions favour an increase of aerosol burdens in the atmosphere due to reduced wet-scavenging, so that in the Indonesian region more

ACPD
12, 5247–5292, 2012

aerosols accumulate. Simultaneously, a change in the wind patterns leads to more effective aerosol transport away from the source regions into the Indian Ocean. Radiative perturbations due to BB aerosols become amplified in both magnitude and extent, but due to the more effective aerosol transport the radiative forcing anomaly appears slightly weakened over some of the major emission regions.

As secondary organic aerosols associated with biomass burning are not considered in this study, our direct forcing anomalies are likely to be underestimated. This is in agreement with satellite-retrieved AODs from MISR and MODIS.

The indirect forcing anomaly showed a similar overall strengthening due to the impact of ENSO-related SST variations. The response of cloud properties to altered meteorological conditions is different compared to the response of the direct forcing, and is not directly linked to the generally increased aerosol burdens and spatial distribution. Our results indicate a strong relationship between the pattern of rainfall changes and aerosol-induced changes of cloud properties. This can be attributed to the dependence of the number of cloud droplets and droplet sizes on the concentration of hydrophilic aerosols. As the latter are effectively washed out by rain, a decrease in rainfall has a positive feedback on the number of cloud droplets. This leads to smaller cloud droplet sizes, which consequently results in a stronger indirect aerosol effect. We compared modelled cloud droplet radii with values from satellite retrievals. The interpretation is difficult, as due to different reference wavelengths different cloud levels are sampled in the retrievals. However, based on the comparison presented here, we conclude that our estimates are reasonable.

Aerosol feedbacks on circulation, as well as the cloud-lifetime effect, are not considered here. These effects could lead to changes in atmospheric dynamics and alter rainfall patterns. As further work, we plan to investigate such feedbacks using a coupled atmosphere-ocean GCM.

Based on the results presented in this study, direct and indirect radiative perturbations from Indonesian BB emissions would be underestimated if feedbacks of ENSO-related SST variations on radiative forcing are not taken into account.

ACPD
12, 5247–5292, 2012

Acknowledgements. We are grateful to Melita Keywood and Mick Meyer for their thoughts and fruitful discussions on this topic and thank Stacey Dravitzki for proof-reading. This work was supported by the NCI National Facility at the ANU.

References

Adler, R. F., Huffman, G. J., Chang, A., Ferraro, R., Xie, P. P., Janowiak, J., Rudolf, B., Schneider, U., Curtis, S., Bolvin, D., Gruber, A., Susskind, J., Arkin, P., and Nelkin, E.: The version-2 global precipitation climatology project (GPCP) monthly precipitation analysis (1979-present), J. Hydromet., 4, 1147–1167, doi:10.1175/1525-7541(2003)004<1147:TVGPCP>2.0.CO;2, 2003. 5258

Chen, W.-T., Kahn, R. A., Nelson, D., Yau, K., and Seinfeld, J. H.: Sensitivity of multiangle imaging to the optical and microphysical properties of biomass burning aerosols, J. Geophys. Res., 113, D10203, doi:10.1029/2007jd009414, 2008. 5260

Cooke, W. F., Liousse, C., Cachier, H., and Feichter, J.: Construction of a 1 degrees x 1 degrees fossil fuel emission data set for carbonaceous aerosol and implementation and radiative impact in the ECHAM4 model, J. Geophys. Res., 104, 22137–22162, doi:10.1029/1999jd900187, 1999. 5252

Davison, P. S., Roberts, D. L., Arnold, R. T., and Colvile, R. N.: Estimating the direct radiative forcing due to haze from the 1997 forest fires in Indonesia, J. Geophys. Res., 109, D10207, doi:10.1029/2003jd004264, 2004. 5249, 5250

Dentener, F., Kinne, S., Bond, T., Boucher, O., Cofala, J., Generoso, S., Ginoux, P., Gong, S., Hoelzemann, J. J., Ito, A., Marelli, L., Penner, J. E., Putaud, J.-P., Textor, C., Schulz, M., van der Werf, G. R., and Wilson, J.: Emissions of primary aerosol and precursor gases in the years 2000 and 1750 prescribed data-sets for AeroCom, Atmos. Chem. Phys., 6, 4321–4344, doi:10.5194/acp-6-4321-2006, 2006. 5252

Duncan, B. N., Bey, I., Chin, M., Mickley, L. J., Fairlie, T. D., Martin, R. V., and Matsueda, H.: Indonesian wildfires of 1997: Impact on tropospheric chemistry, J. Geophys. Res., 108, 4458, doi:10.1029/2002jd003195, 2003. 5249, 5250

Fan, J., Zhang, R., Tao, W.-K., and Mohr, K. I.: Effects of aerosol optical properties on deep convective clouds and radiative forcing, J. Geophys. Res., 113, D08209, doi:10.1029/2007jd009257, 2008. 5269

Feichter, J., Kjellström, E., Rodhe, H., Dentener, F., Lelieveldi, J., and Roelofs, G.-J.: Simulation

ACPD
12, 5247–5292, 2012

of the tropospheric sulfur cycle in a global climate model, Atmos. Environ., 30, 1693–1707, doi:10.1016/1352-2310(95)00394-0, 1996. 5252
Ginoux, P., Chin, M., Tegen, I., Prospero, J. M., Holben, B., Dubovik, O., and Lin, S. J.: Sources and distributions of dust aerosols simulated with the GOCART model, J. Geophys. Res., 106, 20255–20273, doi:10.1029/2000jd000053, 2001. 5253
Gordon, H. B., O'Farrell, S. P., Collier, M. A., Dix, M. R., Rotstayn, L. D., Kowalczyk, E. A., Hirst, A. C., and Watterson, I. G.: The CSIRO Mk3.5 Climate Model, 62 pp., 2010. 5252
Graf, H.-F., Yang, J., and Wagner, T. M.: Aerosol effects on clouds and precipitation during the 1997 smoke episode in Indonesia, Atmos. Chem. Phys., 9, 743–756, doi:10.5194/acp-9-743-2009, 2009. 5269
Gregory, D. and Rowntree, P. R.: A mass flux convection scheme with representation of cloud ensemble characteristics and stability-dependent closure, Mon. Weather Rev., 118, 1483–1506, doi:10.1175/1520-0493(1990)118<1483:AMFCSW>2.0.CO;2, 1990. 5253
Grieshop, A. P., Logue, J. M., Donahue, N. M., and Robinson, A. L.: Laboratory investigation of photochemical oxidation of organic aerosol from wood fires 1: measurement and simulation of organic aerosol evolution, Atmos. Chem. Phys., 9, 1263–1277, doi:10.5194/acp-9-1263-2009, 2009. 5261
Holtslag, A. A. M. and Boville, B. A.: Local versus nonlocal boundary-layer diffusion in a global climate model, J. Climate, 6, 1825–1842, doi:10.1175/1520-0442(1993)006<1825:LVNBLD>2.0.CO;2, 1993. 5253
Huffman, G. J., Adler, R. F., Bolvin, D. T., and Gu, G.: Improving the global precipitation record: GPCP Version 2.1, Geophys. Res. Lett., 36, L17808, doi:10.1029/2009gl040000, 2009. 5258
Hurrell, J. W., Hack, J. J., Shea, D., Caron, J. M., and Rosinski, J.: A new sea surface temperature and sea ice boundary dataset for the Community Atmosphere Model, J. Climate, 21, 5145–5153, doi:10.1175/2008jcli2292.1, 2008. 5254, 5269
Iinuma, Y., Boge, O., Grafe, R., and Herrmann, H.: Methyl-Nitrocatechols: Atmospheric Tracer Compounds for Biomass Burning Secondary Organic Aerosols, Envir. Sci. Technol., 44, 8453–8459, doi:10.1021/es102938a, 2010. 5261
Jones, A., Roberts, D. L., and Slingo, A.: A climate model study of indirect radiative forcing by anthropogenic sulphate aerosols, Nature, 370, 450–453, doi:10.1038/370450a0, 1994. 5253
Kahn, R. A., Gaitley, B. J., Martonchik, J. V., Diner, D. J., Crean, K. A., and Holben, B.: Multiangle Imaging Spectroradiometer (MISR) global aerosol optical depth validation based on

ACPD
12, 5247–5292, 2012

2 years of coincident Aerosol Robotic Network (AERONET) observations, J. Geophys. Res., 110, D10S04, doi:10.1029/2004jd004706, 2005. 5260
King, M. D., Menzel, W. P., Kaufman, Y. J., Tanre, D., Gao, B. C., Platnick, S., Ackerman, S. A., Remer, L. A., Pincus, R., and Hubanks, P. A.: Cloud and aerosol properties, precipitable water, and profiles of temperature and water vapor from MODIS, IEEE Trans. Geosci. Remote Sens., 41, 442–458, doi:10.1109/tgrs.2002.808226, 2003. 5260, 5265
Koch, D. and Del Genio, A. D.: Black carbon semi-direct effects on cloud cover: review and synthesis, Atmos. Chem. Phys., 10, 7685–7696, doi:10.5194/acp-10-7685-2010, 2010. 5269
Lamarque, J.-F., Bond, T. C., Eyring, V., Granier, C., Heil, A., Klimont, Z., Lee, D., Liousse, C., Mieville, A., Owen, B., Schultz, M. G., Shindell, D., Smith, S. J., Stehfest, E., Van Aardenne, J., Cooper, O. R., Kainuma, M., Mahowald, N., McConnell, J. R., Naik, V., Riahi, K., and van Vuuren, D. P.: Historical (1850–2000) gridded anthropogenic and biomass burning emissions of reactive gases and aerosols: methodology and application, Atmos. Chem. Phys., 10, 7017–7039, doi:10.5194/acp-10-7017-2010, 2010. 5252, 5254, 5256
Langmann, B.: A model study of smoke-haze influence on clouds and warm precipitation formation in Indonesia 1997/1998, Atmos. Environ., 41, 6838–6852, doi:10.1016/j.atmosenv.2007.04.050, 2007. 5269
Levine, J. S.: The 1997 fires in Kalimantan and Sumatra, Indonesia: Gaseous and particulate emissions, Geophys. Res. Lett., 26, 815–818, doi:10.1029/1999GL900067, 1999. 5249
Liew, S. C., Lim, O. K., Kwoh, L. K., and Lim, H.: A study of the 1997 forest fires in South East Asia using SPOT quicklook mosaics, Igarss '98 – 1998 International Geoscience and Remote Sensing Symposium, Proceedings Vols 1–5: Sensing and Managing the Environment, Ieee, New York, 1998. 5249
Liu, Y., Daum, P. H., Guo, H., and Peng, Y.: Dispersion bias, dispersion effect, and the aerosol-cloud conundrum, Environ. Res. Lett., 3, 045021, doi:10.1088/1748-9326/3/4/045021, 2008. 5254
Lohmann, U., Feichter, J., Chuang, C. C., and Penner, J. E.: Prediction of the number of cloud droplets in the ECHAM GCM, J. Geophys. Res., 104, 24557–24563, doi:10.1029/1999jd900840, 1999. 5253
Lohmann, U., Rotstayn, L., Storelvmo, T., Jones, A., Menon, S., Quaas, J., Ekman, A. M. L., Koch, D., and Ruedy, R.: Total aerosol effect: radiative forcing or radiative flux perturbation?, Atmos. Chem. Phys., 10, 3235–3246, doi:10.5194/acp-10-3235-2010, 2010. 5255
Louis, J. F.: A parametric model of vertical eddy fluxes in the atmosphere, Bound.-Lay. Meteo-

ACPD
12, 5247–5292, 2012

rol., 17, 187–202, doi:10.1007/bf00117978, 1979. 5253
McGregor, J. L.: Economical Determination of Departure Points for Semi-Lagrangian Models, Mon. Weather Rev., 121, 221–230, doi:10.1175/1520-0493(1993)121<0221:edodpf>2.0.co;2, 1993. 5253
Minnis, P., Sun-Mack, S., Chen, Y., Khaiyer, M. M., Yi, Y., Ayers, J. K., Brown, R. R., Dong, X., Gibson, S. C., Heck, P. W., Lin, B., Nordeen, M. L., Nguyen, L., Palikonda, R., Smith, W. L., Spangenberg, D. A., Trepte, Q. Z., and Xi, B.: CERES Edition-2 Cloud Property Retrievals Using TRMM VIRS and Terra and Aqua MODIS Data – Part II: Examples of Average Results and Comparisons With Other Data, IEEE Trans. Geosci. Remote Sens., PP, 1–30, doi:10.1109/TGRS.2011.2144602, 2011. 5265, 5266
Murdiyarso, D. and Adiningsih, E. S.: Climate anomalies, Indonesian vegetation fires and terrestrial carbon emissions, Mitig. Adapt. Strat. Global Change, 12, 101–112, doi:10.1007/s11027-006-9047-4, 2007. 5249
O'Dowd, C. D., Smith, M. H., Consterdine, I. E., and Lowe, J. A.: Marine aerosol, sea-salt, and the marine sulphur cycle: A short review, Atmos. Environ., 31, 73–80, doi:10.1016/S1352-2310(96)00106-9, 1997. 5252
Ott, L., Duncan, B., Pawson, S., Colarco, P., Chin, M., Randles, C., Diehl, T., and Nielsen, E.: Influence of the 2006 Indonesian biomass burning aerosols on tropical dynamics studied with the GEOS-5 AGCM, J. Geophys. Res., 115, D14121, doi:10.1029/2009jd013181, 2010. 5269
Page, S. E., Siegert, F., Rieley, J. O., Boehm, H. D. V., Jaya, A., and Limin, S.: The amount of carbon released from peat and forest fires in Indonesia during 1997, Nature, 420, 61–65, doi:10.1038/nature01131, 2002. 5249, 5250
Parameswaran, K., Nair, S. K., and Rajeev, K.: Impact of Indonesian forest fires during the 1997 El Nino on the aerosol distribution over the Indian Ocean, Climate Change Processes in the Stratosphere, Earth-Atmosphere-Ocean Systems, and Oceanographic Processes from Satellite Data, 33, 1098–1103, doi:10.1016/S0273-1177(03)00736-1, 2004. 5249
Platnick, S.: Vertical photon transport in cloud remote sensing problems, J. Geophys. Res., 105, 22919–22935, doi:10.1029/2000jd900333, 2000. 5266
Podgorny, I. A., Li, F., and Ramanathan, V.: Large aerosol radiative forcing due to the 1997 Indonesian forest fire, Geophys. Res. Lett., 30, 1028, doi:10.1029/2002gl015979, 2003. 5250
Rajeev, K., Parameswaran, K., Nair, S. K., and Meenu, S.: Observational evidence for the radiative impact of Indonesian smoke in modulating the sea surface temperature of the equatorial

ACPD
12, 5247–5292, 2012

Indian Ocean, J. Geophys. Res., 113, D17201, doi:10.1029/2007jd009611, 2008. 5249, 5268
Ramanathan, V.: Aerosols, Climate, and the Hydrological Cycle, Science, N.Y., 294, 2119–2124, doi:10.1126/science.1064034, 2001. 5250
Remer, L. A., Kaufman, Y. J., Tanre, D., Mattoo, S., Chu, D. A., Martins, J. V., Li, R. R., Ichoku, C., Levy, R. C., Kleidman, R. G., Eck, T. F., Vermote, E., and Holben, B. N.: The MODIS aerosol algorithm, products, and validation, J. Atmos. Sci., 62, 947–973, doi:10.1175/jas3385.1, 2005. 5260
Rotstayn, L. D.: A physically based scheme for the treatment of stratiform clouds and precipitation in large-scale models. I: Description and evaluation of the microphysical processes, Q. J. Roy. Meteorol. Soc., 123, 1227–1282, doi:10.1002/qj.49712354106, 1997. 5253
Rotstayn, L. D. and Liu, Y. G.: Sensitivity of the first indirect aerosol effect to an increase of cloud droplet spectral dispersion with droplet number concentration, J. Climate, 16, 3476–3481, doi:10.1175/1520-0442(2003)016<3476:SOTFIA>2.0.CO;2, 2003. 5254
Rotstayn, L. D. and Liu, Y. G.: A smaller global estimate of the second indirect aerosol effect, Geophys. Res. Lett., 32, L05 708, doi:10.1029/2004gl021922, 2005. 5253
Rotstayn, L. D. and Lohmann, U.: Simulation of the tropospheric sulfur cycle in a global model with a physically based cloud scheme, J. Geophys. Res., 107, 4592, doi:10.1029/2002jd002128, 2002. 5252, 5253, 5264, 5267
Rotstayn, L. D., Cai, W. J., Dix, M. R., Farquhar, G. D., Feng, Y., Ginoux, P., Herzog, M., Ito, A., Penner, J. E., Roderick, M. L., and Wang, M. H.: Have Australian rainfall and cloudiness increased due to the remote effects of Asian anthropogenic aerosols?, J. Geophys. Res., 112, D09202, doi:10.1029/2006jd007712, 2007. 5253
Rotstayn, L. D., Keywood, M. D., Forgan, B. W., Gabric, A. J., Galbally, I. E., Gras, J. L., Luhar, A. K., McTainsh, G. H., Mitchell, R. M., and Young, S. A.: Possible impacts of anthropogenic and natural aerosols on Australian climate: a review, Int. J. Clim., 29, 461–479, doi:10.1002/joc.1729, 2009. 5254, 5255
Rotstayn, L. D., Collier, M. A., Dix, M. R., Feng, Y., Gordon, H. B., O'Farrell, S. P., Smith, I. N., and Syktus, J.: Improved simulation of Australian climate and ENSO-related rainfall variability in a global climate model with an interactive aerosol treatment, Int. J. Clim., 30, 1067–1088, doi:10.1002/joc.1952, 2010. 5252
Rotstayn, L. D., Collier, M. A., Mitchell, R. M., Qin, Y., Campbell, S. K., and Dravitzki, S. M.: Simulated enhancement of ENSO-related rainfall variability due to Australian dust, Atmos.

ACPD
12, 5247–5292, 2012

Chem. Phys., 11, 6575–6592, doi:10.5194/acp-11-6575-2011, 2011. 5253
Saji, N. H., Goswami, B. N., Vinayachandran, P. N., and Yamagata, T.: A dipole mode in the tropical Indian Ocean, Nature, 401, 360–363, doi:10.1038/43855, 1999. 5249
Suzuki, K., Nakajima, T. Y., and Stephens, G. L.: Particle Growth and Drop Collection Efficiency of Warm Clouds as Inferred from Joint CloudSat and MODIS Observations, J. Atmos. Sci., 67, 3019–3032, doi:10.1175/2010jas3463.1, 2010. 5266
Tosca, M. G., Randerson, J. T., Zender, C. S., Flanner, M. G., and Rasch, P. J.: Do biomass burning aerosols intensify drought in equatorial Asia during El Niño?, Atmos. Chem. Phys., 10, 3515–3528, doi:10.5194/acp-10-3515-2010, 2010. 5250
Twomey, S.: Pollution and the planetary albedo, Atmos. Environ., 8, 1251–1256, doi:10.1016/0004-6981(74)90004-3, 1974. 5251
Twomey, S.: The Influence of Pollution on the Shortwave Albedo of Clouds, J. Atmos. Sci., 34, 1149–1152, doi:10.1175/1520-0469(1977)034<1149:TIOPOT>2.0.CO;2, 1977. 5253
van der Werf, G. R., Randerson, J. T., Giglio, L., Collatz, G. J., Mu, M., Kasibhatla, P. S., Morton, D. C., DeFries, R. S., Jin, Y., and van Leeuwen, T. T.: Global fire emissions and the contribution of deforestation, savanna, forest, agricultural, and peat fires (1997–2009), Atmos. Chem. Phys., 10, 11707–11735, doi:10.5194/acp-10-11707-2010, 2010. 5249, 5250, 5252, 5261
van Leer, B.: Towards the ultimate conservative difference scheme. IV. A new approach to numerical convection, J. Comput. Phys., 23, 276–299, doi:10.1016/0021-9991(77)90095-x, 1977. 5253
Webster, P. J., Moore, A. M., Loschnigg, J. P., and Leben, R. R.: Coupled ocean-atmosphere dynamics in the Indian Ocean during 1997–98, Nature, 401, 356–360, doi:10.1038/43848, 1999. 5249
Wielicki, B. A., Barkstrom, B. R., Harrison, E. F., Lee, R. B., Louis Smith, G., and Cooper, J. E.: Clouds and the Earth's Radiant Energy System (CERES): An Earth Observing System Experiment, B. Am. Meteorol. Soc., 77, 853–868, doi:10.1175/1520-0477(1996)077<0853:catere>2.0.co;2, 1996. 5265

ACPD
12, 5247–5292, 2012

Table 1. Key characteristics of the experiments CLIM and AMIP.

Experiment	Indonesian BB emissions		Global SST fields	
	El Niño	La Niña	El Niño	La Niña
CLIM	1997	2000	climatological	
AMIP	1997	2000	1997	2000

ACPD
12, 5247–5292, 2012

Table 2. Pattern correlations describing the relationship between SST-induced changes (AMIP anomaly minus CLIM anomaly) representative for the period July to November. Included variables are the aerosol optical depth (τ_{550}) and small particle aerosol optical depth (τ_{sp}) at 550 nm, burdens of sulfate (SO_4) and organic carbonaceous aerosols (OC), cloud droplet number concentration (N_d) and precipitation (Prec).

	τ_{550}	τ_{sp}	SO_4	OC	N_d	R_e	Prec
τ_{550}	1.0	0.88	0.77	0.76	0.47	−0.38	−0.28
τ_{sp}		1.0	0.77	0.90	0.59	−0.45	−0.37
SO_4			1.0	0.79	0.78	−0.67	−0.62
OC				1.0	0.65	−0.51	−0.49
N_d					1.0	−0.69	−0.67
R_e						1.0	0.61
Prec							1.0

ACPD
12, 5247–5292, 2012

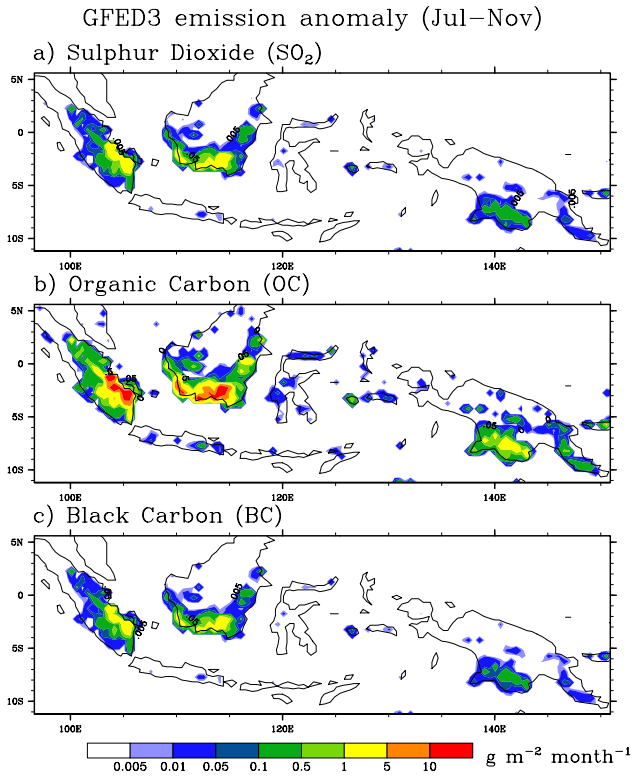

Fig. 1. Average July to November emission anomaly (1997 minus 2000) of sulphur dioxide (SO_2), organic carbon (OC) and black carbon (BC) from the GFED3 database. Units are in gram of the substance per m^2 per month.

ACPD
12, 5247–5292, 2012

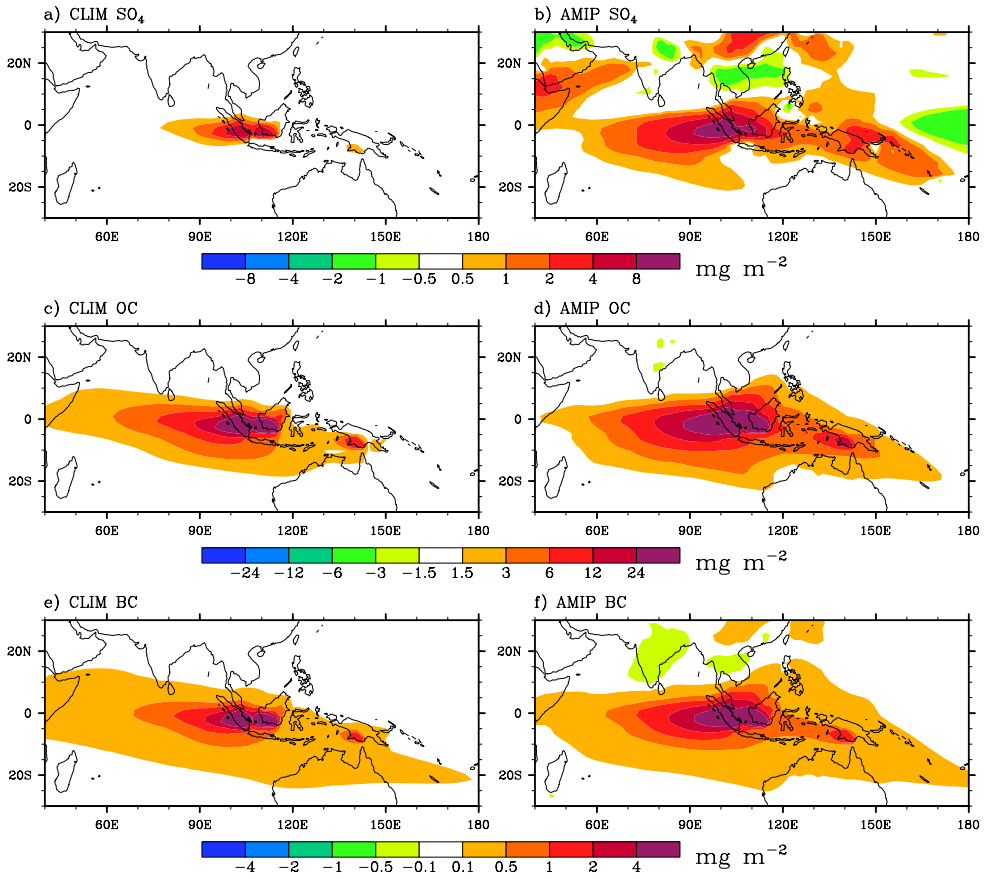

Fig. 2. July to November average of the sulphate (SO_4), organic carbon (OC) and black carbon (BC) burden anomalies (El Niño minus La Niña) from the CLIM (left column) and the AMIP (right column) experiment.

ACPD
12, 5247–5292, 2012

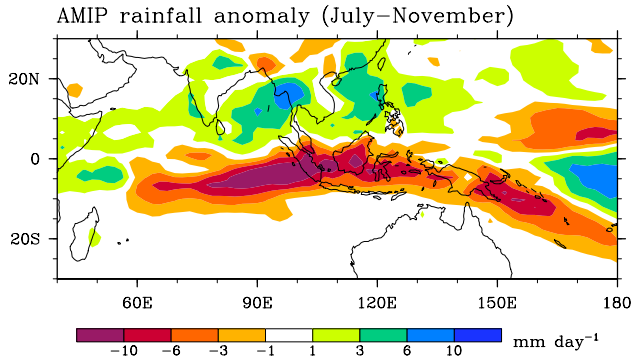

Fig. 3a. SST-induced rainfall anomaly (1997 minus 2000) from the AMIP experiment averaged over the months July to November.

ACPD
12, 5247–5292, 2012

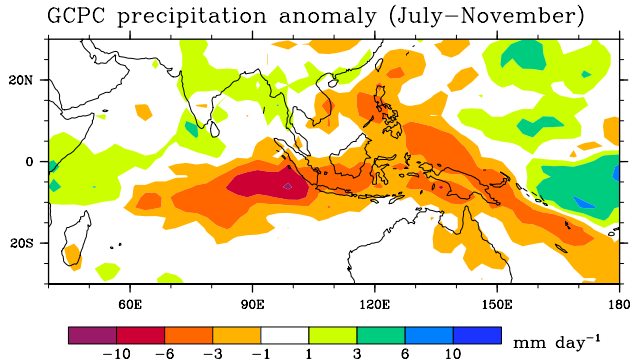

Fig. 3b. July to November average rainfall anomaly (El Niño minus La Niña) based on the year 1997 and year 2000 rainfall from the GPCP dataset.

ACPD
12, 5247–5292, 2012

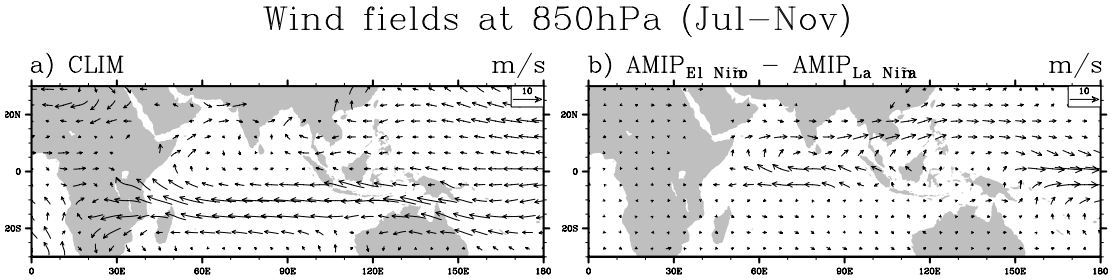

Fig. 4. (a) The mean July to November 850 hPa wind fields that apply for both the El Niño and La Niña cases of the CLIM experiment, and **(b)** the wind anomaly (El Niño minus La Niña) from the AMIP experiment averaged over the same months.

ACPD
12, 5247–5292, 2012

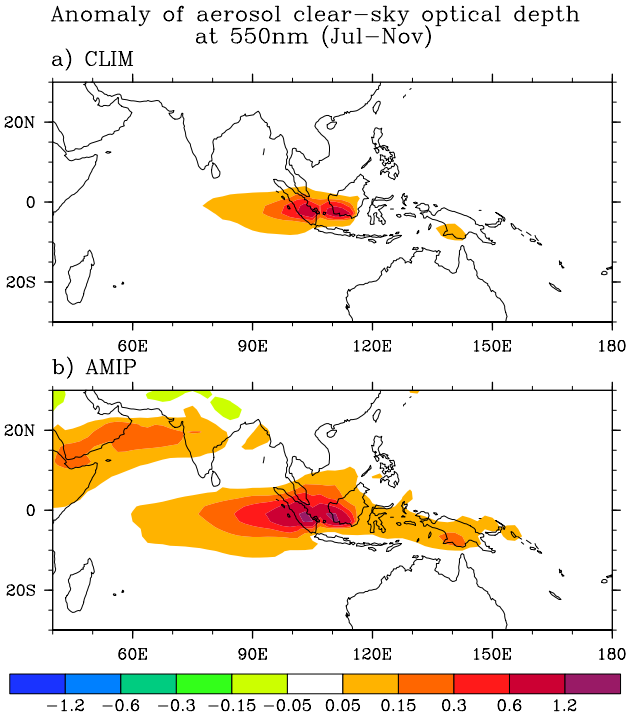

Fig. 5. Anomaly (El Niño minus La Niña) of aerosol clear-sky optical depth at 550 nm from the **(a)** CLIM and the **(b)** AMIP experiment averaged for the period July to November.

ACPD
12, 5247–5292, 2012

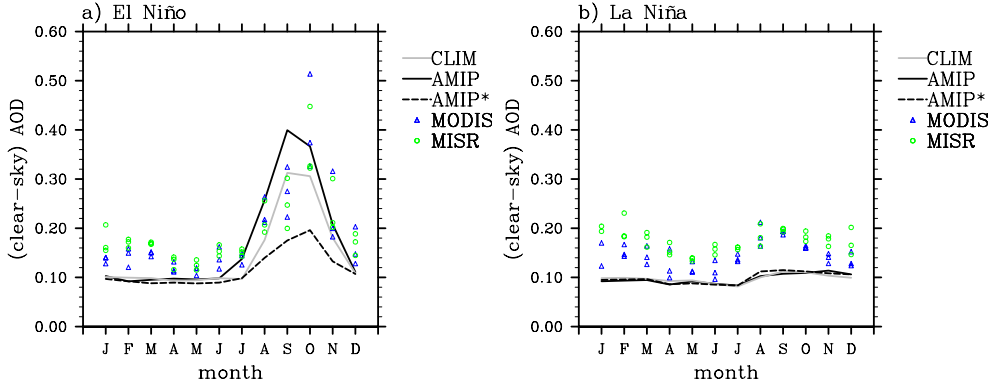

Fig. 6. Aerosol optical depths (AODs) at 550 nm of CLIM (grey), AMIP (black, solid line) and AMIP* (black, dashed line) representing average **(a)** El Niño and **(b)** La Niño conditions over the Indonesian region (5.6° N–11.2° S, 96.6° E–150.9° E) in comparison with MODIS (blue triangle) and MISR (green circle) measurements. AODs from the CLIM and AMIP experiment simulate the year-1997 El Niño and the year-2000 La Niña. The satellite retrievals MODIS and MISR are from the El Niño years 2002, 2004 and 2006 and the La Niña years 2000, 2001 and 2005, respectively. AMIP* represents monthly mean AODs based on the same years as the satellite data.

ACPD
12, 5247–5292, 2012

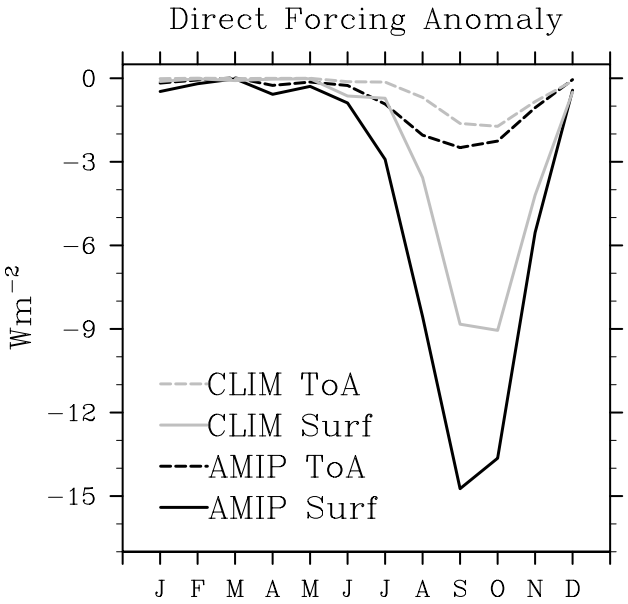

Fig. 7. Direct forcing anomaly (El Niño minus La Niña) for the Indonesian region (5.6° N–11.2° S, 96.6° E–150.9° E) at the top of atmosphere (dashed) and the surface (solid) from the CLIM (grey) and AMIP (black) experiment.

ACPD
12, 5247–5292, 2012

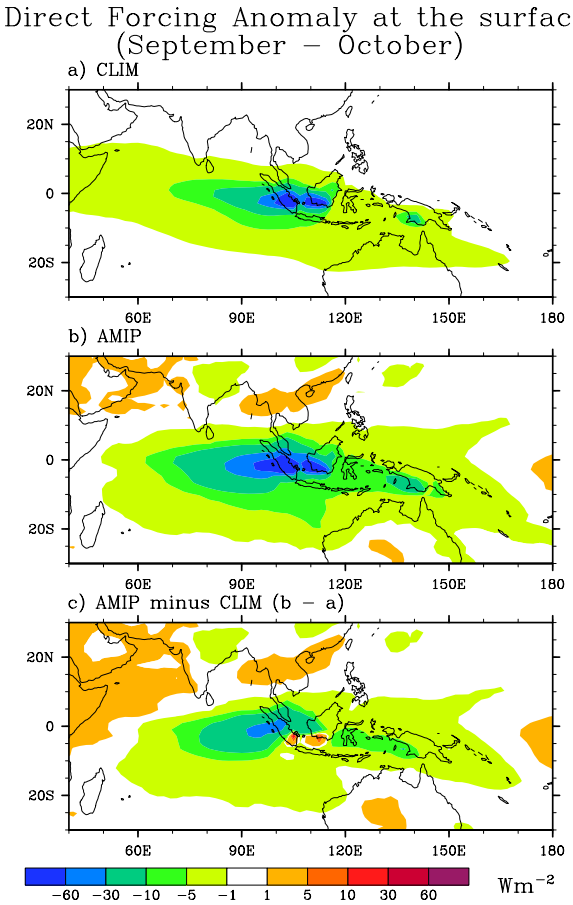

Fig. 8. Average September–October direct forcing anomaly (El Niño minus La Niña) from **(a)** the CLIM and **(b)** AMIP experiment and **(c)** the difference between AMIP and CLIM.

ACPD
12, 5247–5292, 2012

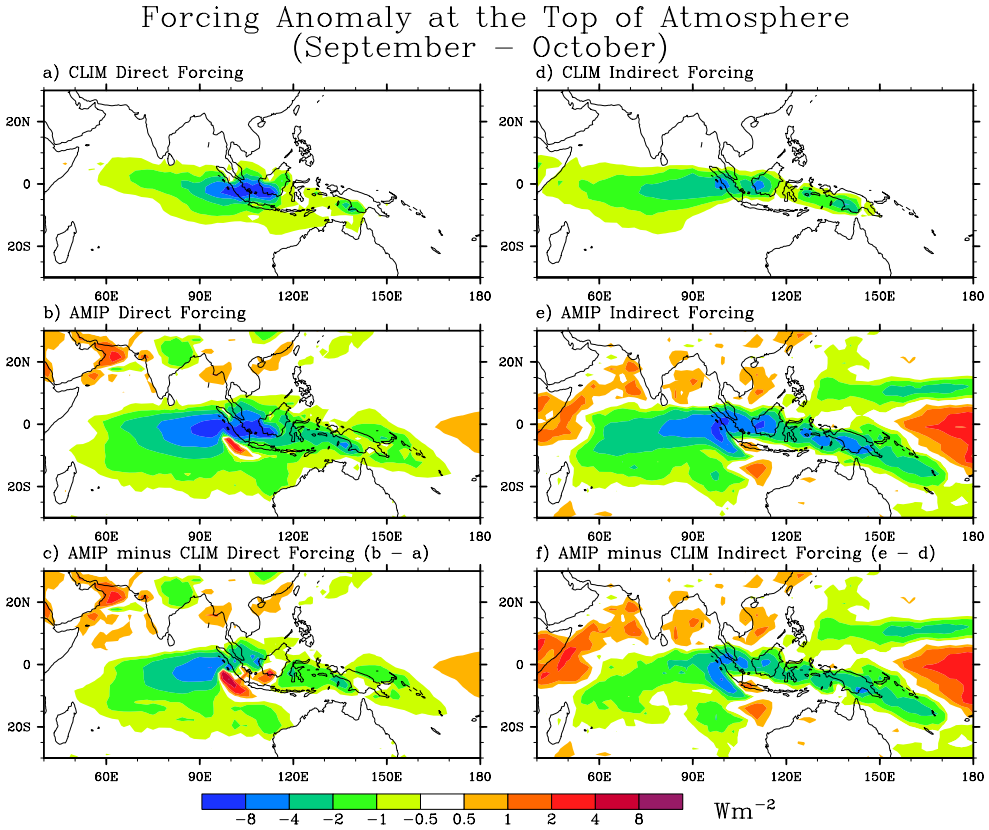

Fig. 9. Average September–October direct (left column) and indirect (right column) forcing anomaly (El Niño minus La Niña) from the CLIM (top) and AMIP (middle) experiment and the difference between AMIP and CLIM (bottom).

ACPD
12, 5247–5292, 2012

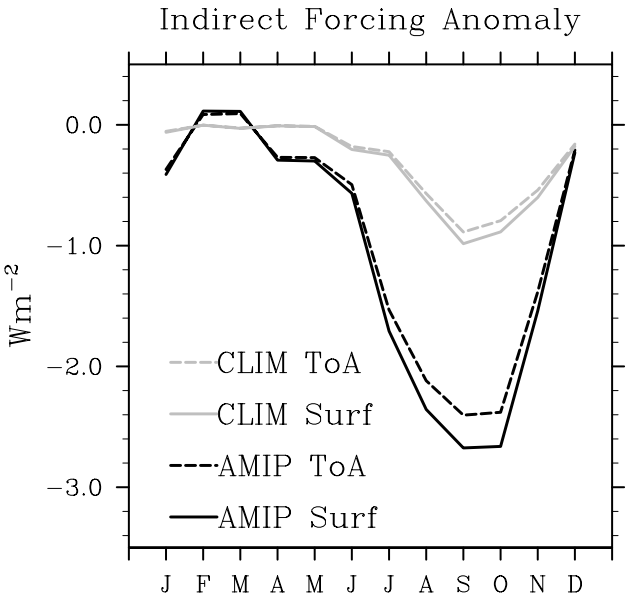

Fig. 10. Indirect forcing anomaly (El Niño minus La Niña) for the Indonesian region (5.6° N–11.2° S, 96.6° E–150.9° E) at the top of atmosphere (dashed) and the surface (solid) from the CLIM (grey) and AMIP (black) experiment.

ACPD
12, 5247–5292, 2012

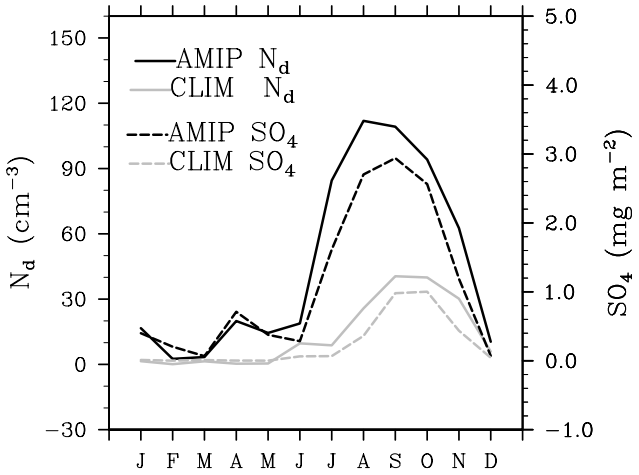

Fig. 11. Monthly anomaly (El Niño minus La Niña) of the cloud droplet number concentration (N_d in cm^{-3}, solid lines) and sulphate burdens (SO_4 in $mg\,m^{-2}$, dashed lines) within the Indonesian region (5.6° N–11.2° S, 96.6° E–150.9° E) of the CLIM (grey) and the AMIP (black) experiment.

ACPD
12, 5247–5292, 2012

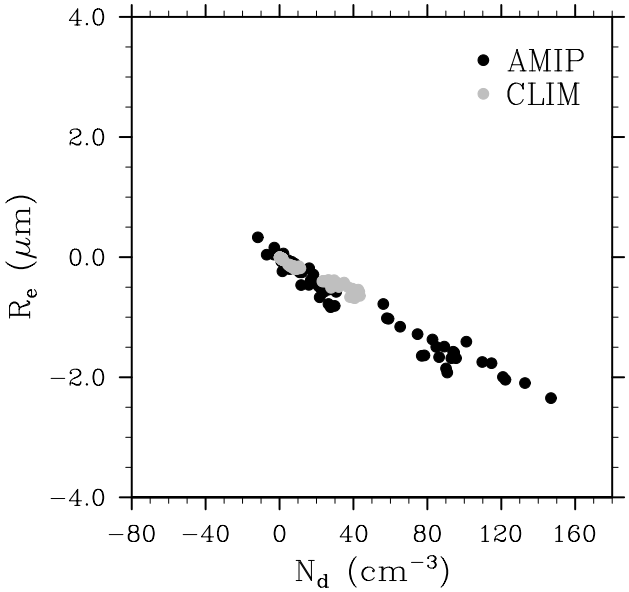

Fig. 12. Monthly anomaly (El Niño minus La Niña) of the cloud effective radius (R_e in µm) for the Indonesian region (5.6° N–11.2° S, 96.6° E–150.9° E) as a function of the monthly anomaly of the cloud droplet number concentration (N_d in cm^{-3}) for each ensemble member of the CLIM (grey) and AMIP (black) experiment.

ACPD
12, 5247–5292, 2012

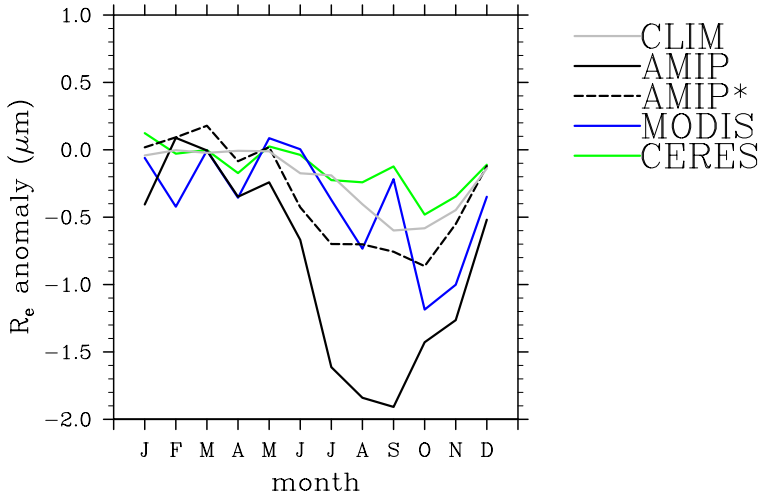

Fig. 13. Comparison of the monthly cloud effective radius (R_e) anomaly (El Niño minus La Niña) within the Indonesian region (5.6° N–11.2° S, 96.6° E–150.9° E) from the AMIP (black, solid), AMIP* (black, dashed) and CLIM (grey) experiment with satellite retrievals from MODIS (blue) and CERES (green). The anomaly of AMIP and CLIM are based on the El Niño and La Niña years 1997 and 2000, respectively. The anomalies of the satellite retrievals as well as of AMIP* are based on the El Niño years 2002, 2004 and 2006 and the La Niña years 2000, 2001 and 2005.

ACPD
12, 5247–5292, 2012